NUMERICAL INVESTIGATION OF THE SQUEEZING FLOW OF TERNARY HYBRID NANOFLUID $(Cu - Al_2O_3 - TiO_2/H_2O)$ BETWEEN TWO PARALLEL PLATES IN A DARCY POROUS MEDIUM WITH VISCOUS DISSIPATION AND HEAT SOURCE

 Rubul Bora, Bidyut Boruah*

Department of Mathematics, CNB College, Bokakhat-785612, Assam, India
*Corresponding Author e-mail: rubulboracnbc@gmail.com

This work aims to investigate numerically the influence of viscous dissipation and heat source on the magnetohydrodynamics squeezing flow of water-based ternary hybrid nanofluids between two parallel plates in a Darcy porous medium. The nanoparticles Cu, Al_2O_3, and TiO_2 are dispersed in a base fluid H_2O, resulting in the creation of a ternary hybrid nanofluid $Cu - Al_2O_3 - TiO_2/H_2O$. This study examines the deformation of the lower plate as the upper one advances towards it. The numerical results are computed using the 3-stage Lobatto IIIa method, which is specially implemented by Bvp4c in MATLAB. The effects of various parameters are visually illustrated through graphs and quantitatively shown in tables. The absolute skin friction of the ternary hybrid nanofluid is seen to be approximately 5% higher than that of the regular nanofluid at the lower plate and at most 7% higher than that of the nanofluid at the upper plate. The heat transmission rate of the ternary hybrid nanofluid is higher at the upper plate compared to the lower plate.

Keywords: *Thermal radiation; Viscous dissipation; Parallel plate; Heat source; Ternary hybrid nanofluid; Darcy porous medium; bvp*

PACS: 44.05.+e, 44.25.+f, 44.27.+g, 44.40.+a, 47.11.-j, 44.30.+v

1. INTRODUCTION

Ternary hybrid nanofluids consist of three distinct kinds of nanoparticles dispersed in a base fluid. This paper describes a study on a ternary hybrid nanofluid consisting of copper (Cu), aluminum oxide (Al_2O_3), and titanium dioxide (TiO_2) nanoparticles, which are uniformly dispersed in a water-based fluid. This ternary hybrid nanofluid possesses distinctive characteristics that enable it suited for a many different kinds of applications. Introducing copper (Cu) nanoparticles into the nanofluid has been discovered to enhance thermal conductivity, while the inclusion of aluminum oxide (Al_2O_3) and titanium dioxide (TiO_2) nanoparticles has been reported to improve heat transfer efficiency and stability. This nanofluid can be used in a range of applications, including heat exchangers, cooling systems, and electronic devices, to improve heat dissipation and enhance thermal management. Copper nanoparticles exhibit antibacterial properties, while (TiO_2) nanoparticles demonstrate photocatalytic activity against bacteria and other microorganisms. The utilization of the ternary hybrid nanofluid, consisting of $Cu - Al_2O_3 - TiO_2$, has great potential for creating antibacterial coatings on different surfaces, such as textiles, medical equipment, and food packaging. These coatings efficiently hinder bacterial proliferation and help maintain hygiene. Titanium dioxide (TiO_2) nanoparticles possess photocatalytic characteristics, enabling them to effectively catalyze the decomposition of organic pollutants and the sterilization of water. The utilization of the $Cu - Al_2O_3 - TiO_2$, ternary hybrid nanofluid shows promise for implementation in water treatment processes, aiding in the removal of contaminants and improving the overall water quality.

Choi and Eastman [1] were the innovators who first introduced the concept of nanofluids. They claimed that by suspending metallic nanoparticles in conventional heat transfer fluids, a groundbreaking kind of heat transmission fluids might be created. Raees et al. [2] has conducted an investigation of the unsteady squeezing flow of fluid between parallel plates that contains both nanoparticles and gyrotactic microorganisms, one of the plates was moving and the other staying still. Hayat et al. [3] applied the HAM approach to study the magnetohydrodynamic squeezing flow of a nanofluid across a porous stretched surface with thermophoresis effects and Brownian motion. They have taken the lower wall of the channel to be permeable and stretched, while the upper impermeable wall moves in the direction of the lower wall at a prescribed time-dependent velocity. Moreover, Hayat et al. [4] discovered a novel analysis of the magnetohydrodynamic squeezing flow of couple stress nanomaterial between two parallel surfaces. This analysis incorporates the unique characteristics of thermophoresis and Brownian motion, which have not been previously described together with a porous lower surface in the channel. Salehi et al. [5] has conducted research on the magnetohydrodynamic squeezing nanofluid flow of hybrid nanoparticles composed of Fe_3O_4 and MoS_2 that are sandwiched between two infinite parallel plates. They found that as the squeezing and Hartman numbers increased, the velocity profile decreased. Acharya [6] performed research to determine the flow patterns and heat transmission characteristics of hybrid nano liquids in the presence of nonlinear solar radiation. The investigation focused on several solar thermal devices that had Alumina-copper nano ingredients mixed with water as the main fluid. Furthermore, Bio-convective nano liquid flow including gyrotactic microorganisms between two squeezed parallel plates was investigated by Acharya et al. [7] using the classical Runge-Kutta-Fehlberg approach, taking

into account the effects of a higher-order chemical reaction and second-order slip. Based on their research, they discovered that the temperature reduces as the squeezing factor and first-order velocity slip parameter increase, but increases as the second-order slip parameter increases. A micro-polar hybrid nanofluid ($GO - Cu/H_2O$) has been investigated by Ikram et al. [8] in the presence of hall current and thermal radiations to look at how it moves and transfers heat between two surfaces in a spinning system. The primary result of their investigation is that increasing the values of the magnetic parameter leads to an increase in the velocity profile and a decrease in the rotational velocity profile. Also, the fractional model of Brinkman type fluid that contains hybrid nanoparticles of TiO_2 and Ag in a base fluid of water within a confined micro-channel has been investigated by Ikram et al. [9]. Khashi'ie et al. [10] investigated the $Cu - Al_2O_3/H_2O$ nanofluid flow between two parallel plates in which a magnetic field and wall mass suction or injection are supplied to the lower plate, allowing the bottom plate to be deformed while the upper plate flows in the opposite direction of the lower plate. The primary finding of their investigation is that an augmentation in the squeezing parameter leads to a degradation of the heat transfer coefficient by 4.28% (upper) and 5.35% (lower), respectively. Yaseen et al. [11] studied the heat transfer properties of the MHD squeezing nanofluid (MoS_2/H_2O) flow and the hybrid nanofluid ($MoS_2 - SiO_2/H_2O - C_2H_6O_2$) flow between two parallel plates, as well as their symmetrical characteristics. In their model, the upper plate is moving downwards towards the lower plate, while the bottom plate is elongating with a constant velocity. A hybrid nanofluid containing Ethylene glycol-water as the base fluid and nanoparticles of TiO_2 and MoS_2 in the presence of dust particles and a magnetic field, flowing over a stretched sheet, was studied by Talebi et al. [12] in terms of its motion and temperature distribution in a porous medium. By considering the effects of thermal radiation and Hall current, Rauf et al. [13] investigated the micropolar tri-hybrid nanofluid($Fe_3O_4 - Al_2O_3 - TiO_2/H_2O$) in a rotating structure between two perpendicular permeable plates. A micro-polar fluid undergoing radiative and magnetohydrodynamic flow across an Al_2O_3 and Cu nanoparticle stretched/shrinking sheet in the presence of viscous dissipation and Joule heating was investigated by Waini et al. [14]. Famakinwa et al. [15] studied how heat radiation and viscous dissipation affect an unstable, incompressible flow of water-hybrid nanoparticles moving between two surfaces that are lined up and have different viscosity. They discovered that there was no apparent alteration in fluid velocity when thermal radiation and viscous dissipation parameters were increased, but that the temperature distribution was reduced. The combined effects of the suction/injection, electromagnetic force, activation energy, chemical reaction, ionized fluid, inertia force and magnetic field that influence the squeezing flow of ternary hybrid nanofluids between parallel plates are investigated numerically by Bilal et al. [16]. Hanif et al. [17] investigated the flow of a hybrid nanofluid based on an aluminum alloy and water across a stretchy horizontal plate with a thermal resistive effect using the Numerical Crank-Nicolson approach. The MHD flow, heat, and mass transfer of the Jeffrey hybrid nanofluid on the squeezing channel via a permeable material in the presence of a chemical reaction and a heat sink/source were studied by Noor and Shafie [18]. Ullah et al. [19] explored the hydrothermal properties of a hybrid nanofluid ($Ag + TiO_2 + H_2O$) in three dimensions in presence of magnetic, thermal, and radiation fluxes between the two vertical plates. Transient free convection of a hybrid nanofluid between two parallel plates in the presence of a magnetic field, a heat source/sink and thermal radiation was explored analytically by Roy and Pop [20]. Moreover, the effect of radiative heat flux on the transient state electro-osmotic squeezing propulsion of a viscous liquid via a porous material between two parallel plates has been investigated by Jayavel et al. [21]. Bhaskar et al. [22] and Maiti and Mukhopadhyay [23] investigated the MHD squeezed flow of casson hybrid nanofluid and unstable nanofluid flow between two parallel plates, respectively, under various effects. Madit et al. [24] studied how a chemical reaction affects the flow of a nanofluid that is squeezed by hydromagnetism between two vertical plates. Khashi'ie et al. [25] carried out investigations into the simultaneous impact of double stratification and buoyancy forces on the flow of nanofluid over a surface that is either shrinking or stretching. It was observed that the heat transfer rate increases by roughly 5.83% to 12.13% when the thermal relaxation parameter is introduced in both shrinking and stretching scenarios. Similarly, Khashi'ie et al. [26] developed numerical solutions and conducts stability analyses for stagnation point flow utilizing hybrid nanofluid in the presence of thermal stratification across a permeable stretching/shrinking cylinder. Nath and Deka [27] studied the effects of thermal and mass stratification on an unsteady MHD nanofluid past a vertical plate that accelerates exponentially with temperature variation in a porous media. Similarly, Nath and Deka [28] conducted a numerical study to examine the combined impacts of thermal and mass stratification on the movement of unstable magnetohydrodynamic nanofluid through an exponentially accelerated vertical plate in a porous media. The unsteady parabolic flow across an infinite vertical plate with exponentially declining temperature and variable mass diffusion in a porous media has been investigated by Nath and Deka [29] with respect to the thermal and mass stratification effect. Nath and Deka [30],[31] performed a numerical investigation on the MHD ternary hybrid nanofluid around a vertically stretching cylinder in a porous medium with thermal stratification. A numerical study was carried out by Krishna [32] to examine the effects of heat absorption and generation on steady free convection flow around a perpendicularly wavy surface. Additionally, Krishna and Vajravelu [33] investigated the chemical reaction, radiation absorption, Hall, and ion slip impacts in the rotating MHD flow of second-grade fluid via a porous media between two vertical plates. In a parallel plate channel with different pressure gradient oscillations, Krishna [34] investigated Hall effects on magnetohydrodynamic rotational flow through a porous media.

Based on the literature review, previous research has not attempted to investigate the squeezing flow of an MHD ternary hybrid nanofluid between two parallel plates in a porous media in presence of viscous dissipation effect. It is assumed that the lower plate has a physically permeable and stretchable shape. The primary aim of this study is to investigate the thermal conductivity characteristics of a ternary hybrid nanofluid composed of $Cu - Al_2O_3 - TiO_2$ particles

suspended in water. This study examines the heat transfer characteristics between two parallel plates, considering the influence of thermal radiation as well as heat sources/sinks. The bvp4c solver in MATLAB is used to transform the non-linear PDEs into ODEs by utilizing the necessary self-similarity variables. The Bvp4c technique employed in this research work to represent the problem is generally acknowledged, as evidenced by its discussion and implementation in MATLAB by Hale and Moore [35]. A visual depiction of the outcomes is presented for many parameters, including $\delta, Ec, Sq, S, \lambda, M, Da, R$ and Q.
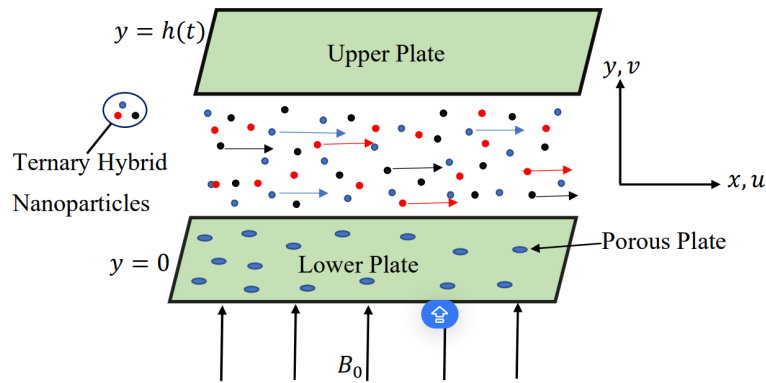
Figure 1. Physical Model and Coordinate System

2. MATHEMATICAL ANALYSIS

Consider a two-dimensional unsteady ternary hybrid nanofluid ($Cu - Al_2O_3 - TiO_2/H_2O$) squeezing flow between two infinite parallel plates in a Darcy porous medium, as illustrated in Fig. 1. The upper plate is positioned at a distance of $y = h(t) = \sqrt{\frac{(1-\alpha t)v_f}{b}}$ from the lower plate. At the same time, the higher plate, with a velocity $V_h = \frac{dh(t)}{dt} = -\frac{\alpha}{2}\sqrt{\frac{v_f}{(1-\alpha t)b}}$, is moving towards the lower plate that is being squeezed. It is assumed that the lower and upper plates are kept at constant temperatures T_1 and T_2, respectively. Additionally, the influence of viscous dissipation, thermal radiation and heat source/sink are taken into consideration in this model; however, the buoyancy effect, which is also known as the gravitational force, is not taken into account. In the meantime, the physical representation for the potential fluid suction or injection includes the porous lower plate, where the wall mass velocity is represented as $v_w = -\frac{V_0}{1-\alpha t}$; for suction, $V_0 > 0$, for injection, $V_0 < 0$, and an impermeable plate corresponds to $V_0 = 0$. Furthermore, the lower plate can be stretched with a linear velocity of $u_w = -\frac{bx}{1-\alpha t}$, where $t < \frac{1}{\alpha}$, and a time-dependent magnetic field is modeled with $B(t) = \frac{B_0}{1-\alpha t}$. In light of these assumptions and with the hybrid nanofluid model that Khashi'ie et al. [10], Famakinwa et al. [15] and Yaseen et al. [11] have proposed, we extended their model to incorporate the ternary hybrid model. Hence, the governing conservation equations are as follows:

$$\frac{\partial u}{\partial x} + \frac{\partial u}{\partial y} = 0 \tag{1}$$

$$\frac{\partial V}{\partial t} + u\frac{\partial V}{\partial x} + v\frac{\partial V}{\partial y} = \frac{\mu_{thnf}}{\rho_{thnf}}\frac{\partial^2 V}{\partial y^2} - \frac{\sigma_{thnf}}{\rho_{thnf}}B(t)^2 V - \frac{\mu_{thnf}}{\rho_{thnf}}\cdot\frac{\phi^* V}{k_p} \tag{2}$$

$$\frac{\partial T}{\partial t} + u\frac{\partial T}{\partial x} + v\frac{\partial T}{\partial y} = \frac{k_{thnf}}{(\rho c_p)_{thnf}}\frac{\partial^2 T}{\partial y^2} - \frac{1}{(\rho c_p)_{thnf}}\frac{\partial q_r}{\partial y} + \frac{Q_0}{(\rho c_p)_{thnf}}(T - T_0) + \frac{\mu_{thnf}}{(\rho c_p)_{thnf}}\left(\frac{\partial u}{\partial y}\right)^2 \tag{3}$$

where $V = \frac{\partial v}{\partial x} - \frac{\partial u}{\partial y}$. The boundary conditions that are associated with the lower and upper plates (Hayat et al. [3] and Khashi'ie et al. [10]) are as follows :

$$u = \lambda\frac{bx}{1-\alpha t} \qquad v = -\frac{V_0}{1-\alpha t} \qquad T = T_1 \qquad\qquad \text{at } y = 0 \text{ (lower plate)}$$

$$u = 0 \qquad\qquad v = \frac{dh(t)}{dt} \qquad T = T_2 \qquad\qquad \text{at } y = h(t) \text{ (upper plate)}$$

Here, u and v represent the velocities in the x and y directions, respectively, while T denotes the temperature of the ternary hybrid nanofluid. In addition, the other symbol signifies the following: ρ represents density, μ represents dynamic viscosity, C_p represents heat capacity, k represents thermal conductivity, $B(t)$ represents magnetic field strength, indicates

porosity of the porous medium, represents permeability of the porous medium, λ is the stretching/shrinking parameter, Q_0 represents heat absorption/generation coefficient, and b denotes the stretching/shrinking rate of the lower plate.

Taking into consideration the Rosseland approximation [36], the value of (q_r) is defined as

$$q_r = -\frac{4\sigma^*}{3k_{thnf}}\left(\frac{\partial T^4}{\partial y}\right)$$

The term "σ^*" represents the Stefan-Boltzmann constant, whereas "k_{thnf}" refers to the mean absorption coefficient. By performing basic calculations with the aforementioned term, Eqn. (3) can be reduced as follows:

$$\frac{\partial T}{\partial t} + u\frac{\partial T}{\partial x} + v\frac{\partial T}{\partial y} = \frac{1}{(\rho c_p)_{thnf}}\left(k_{thnf} + \frac{16\sigma^*T_2^3}{3k}\right)\frac{\partial^2 T}{\partial y^2} + \frac{Q_0}{(\rho c_p)_{thnf}}(T - T_0) + \frac{\mu_{thnf}}{(\rho c_p)_{thnf}}\left(\frac{\partial u}{\partial y}\right)^2$$

The similarity transformation (Ref. Hayat et al. [3]) used in Equations (1)-(3) are as follows

$$u = \frac{bx}{1 - \alpha t}f'(\eta), \quad v = -\sqrt{\frac{b\nu_f}{1 - \alpha t}}f'(\eta), \quad \eta = y\sqrt{\frac{b}{(1 - \alpha t)\nu_f}},$$

$$\psi = \sqrt{\frac{b\nu_f}{1 - \alpha t}}xf(\eta), \quad \theta = \frac{T - T_0}{T_2 - T_0}$$

and we provide non-dimensional quantities in the following:

$$M = \frac{\sigma_f B_0^2}{b\rho_f}, \quad Da = \frac{k_0 b}{\nu_f(1 - \alpha t)\phi^*}, \quad Ec = \frac{u_w^2}{C_p(T_2 - T_0)}, \quad Sq = \frac{\alpha}{b}, \quad S = \frac{V_0}{hb}$$

$$\delta = \frac{T_1 - T_0}{T_2 - T_0}, \quad Q = \frac{Q_0}{1 - \alpha t}, \quad R = \frac{4\sigma^*T_2'^3}{k_f k}, \quad Pr = \frac{(\rho c_p)_f}{k_f}$$

where, M is the magnetic parameter, Da is the Darcy number, Sq is the squeezing parameter, S is the suction/injection parameter, δ is the temperature-ratio parameter, Ec is the Eckert number, Q is the heat source/sink parameter, R is the thermal radiation parameter, Pr is the Prandtl number. Moreover, if $\lambda = 0$, it means the lower plate is not moving, if $\lambda < 0$, it means the lower plate is shrinking, and if $\lambda > 0$, it means the lower plate stretching.

The non-dimensional forms of the transformed equations are given by

$$a_1 a_2 f^{iv} + ff''' - f'f'' - \frac{Sq}{2}(3f'' + \eta f''') - \left(a_2 a_3 M + \frac{a_1 a_2}{Da}\right)f'' = 0 \qquad (4)$$

$$\frac{a_4}{Pr}\left(a_5 + \frac{4}{3}R\right)\theta'' + f\theta' - \frac{Sq}{2}\eta\theta' + a_4 Q\theta + a_1 a_4 Ec f''^2 = 0 \qquad (5)$$

where,

$$a_1 = \frac{\mu_{thnf}}{\mu_f}, \quad a_2 = \frac{\rho_f}{\rho_{thnf}}, \quad a_3 = \frac{\sigma_{thnf}}{\sigma_f}, \quad a_4 = \frac{(\rho C_p)_f}{(\rho C_p)_{thnf}}, \quad a_5 = \frac{k_{thnf}}{k_f}$$

Here, the symbols $\mu_{thnf}, \rho_{thnf}, (\rho C_p)_{thnf}, \sigma_{thnf}, k_{thnf}$ represent the ternary hybrid nanofluid's coefficient of viscosity, electrical conductivity, heat capacity, density and thermal conductivity, respectively. Also, $\mu_f, \rho_f, (\rho C_p)_f, \sigma_f, k_f$ denote the base fluid's coefficient of viscosity, electrical conductivity, heat capacity, density and thermal conductivity correspondingly. The thermophysical characteristics of the ternary hybrid nanofluid are presented in table 1. Thermo-physical properties of Cu, Al_2O_3 and TiO_2 nanoparticles in pure water are given in table 2.

The transformed boundary conditions are as follows :

$$f(0) = S, \qquad\qquad f'(0) = \lambda, \qquad\qquad \theta(0) = \delta$$

$$f(1) = \frac{Sq}{2}, \qquad\qquad f'(1) = 0, \qquad\qquad \theta(1) = 1 \qquad (6)$$

where ϕ_1, ϕ_2 and ϕ_3 are volume fraction of Cu(Copper), Al_2O_3 (aluminium oxide) and TiO_2 (titanium oxide) nanoparticles respectively. The suffixes thnf, hnf, nf, f, s1, s2, s3 denote ternary hybrid nanofluid, hybrid nanofluid, nanofluid, base fluid, solid nanoparticles of copper (Cu), aluminum oxide (Al_2O_3), and titanium dioxide (TiO_2) correspondingly.

The skin friction coefficient and local Nusselt number at lower and upper plates are defined by

$$\text{Lower: } C_{f_1}Re_x^{1/2} = \frac{\mu_{thnf}}{\mu_f}f''(0) \quad\text{and}\quad \text{Upper: } C_{f_2}Re_x^{1/2} = \frac{\mu_{thnf}}{\mu_f}f''(1)$$

$$\text{Lower: } Nu_{x_1}Re_x^{-1/2} = -\left(\frac{k_{thnf}}{k_f} + \frac{4}{3}R\right)\theta'(0) \quad\text{and}\quad \text{Upper: } Nu_{x_2}Re_x^{-1/2} = -\left(\frac{k_{thnf}}{k_f} + \frac{4}{3}R\right)\theta'(1)$$

where, $Re_x = \frac{xU_w}{\nu_f}$ is the local Reynolds Number.

Table 1. The thermo-physical properties of ternary hybrid nanofluid are as follows [31]:

Properties	Ternary Hybrid Nanofluid
Dynamic Viscocity	$\dfrac{\mu_{thnf}}{\mu_f} = \dfrac{1}{(1-\phi_1)^{2.5}(1-\phi_2)^{2.5}(1-\phi_3)^{2.5}}$
Density	$\rho_{thnf} = (1-\phi_3)\left[(1-\phi_2)\left\{(1-\phi_1)\rho_f + \phi_1\rho_{s1}\right\} + \phi_2\rho_{s2}\right] + \phi_3\rho_{s3}$
Electrical Conductivity	$\sigma_{thnf} = \left[\dfrac{(\sigma_{s3}+2\sigma_{hnf})-2\phi_3(\sigma_{hnf}-\sigma_{s3})}{(\sigma_{s3}+2\sigma_{hnf})+\phi_3(\sigma_{hnf}-\sigma_{s3})}\right]\sigma_{hnf}$ $\sigma_{hnf} = \left[\dfrac{(\sigma_{s2}+2\sigma_{nf})-2\phi_2(\sigma_{nf}-\sigma_{s2})}{(\sigma_{s2}+2\sigma_{nf})+\phi_2(\sigma_{nf}-\sigma_{s2})}\right]\sigma_{nf}$ $\sigma_{nf} = \left[\dfrac{(\sigma_{s1}+2\sigma_f)-2\phi_1(\sigma_f-k_{s1})}{(\sigma_{s1}+2\sigma_f)+\phi_1(\sigma_f-\sigma_{s1})}\right]\sigma_f$
Heat Capacity	$(\rho c_p)_{thnf} = (1-\phi_3)\left[(1-\phi_2)\left\{(1-\phi_1)(\rho c_p)_f + \phi_1(\rho c_p)_{s1}\right\}\right.$ $\left. +\phi_2(\rho c_p)_{s2}\right] + \phi_3(\rho c_p)_{s3}$
Thermal Conductivity	$k_{thnf} = \left[\dfrac{(k_{s3}+2k_{hnf})-2\phi_3(k_{hnf}-k_{s3})}{(k_{s3}+2k_{hnf})+\phi_3(k_{hnf}-k_{s3})}\right]k_{hnf}$ $k_{hnf} = \left[\dfrac{(k_{s2}+2k_{nf})-2\phi_2(k_{nf}-k_{s2})}{(k_{s2}+2k_{nf})+\phi_2(k_{nf}-k_{s2})}\right]k_{nf}$ $k_{nf} = \left[\dfrac{(k_{s1}+2k_f)-2\phi_1(k_f-k_{s1})}{(k_{s1}+2k_f)+\phi_1(k_f-k_{s1})}\right]k_f$

Table 2. Thermo-physical Properties of water and nanoparticles [31]

Physical Properties	H_2O(base fluid)	Cu (s1)	Al_2O_3 (s2)	TiO_2 (s3)
$\rho\ (kg/m^3)$	997.1	8933	3970	4250
$C_p\ (J/kgK)$	4179	385	765	686.2
$k\ (W/mK)$	0.613	401	40	8.9538
$\sigma\ (s/m)$	5.5×10^{-6}	59.6×10^6	35×10^6	2.6×10^6

3. METHOD OF SOLUTION

In order to obtain numerical solutions for a system of higher-order nonlinear ordinary differential equations (ODEs) provided by Eqs. (4) and (5) and the boundary conditions, we use the bvp4c solver, built into the computational platform MATLAB. Professionals and researchers have widely employed this technique for solving fluid flow problems. The bvp4c solver, developed by Jacek Kierzenka and Lawrence F. Shampine from Southern Methodist University in Texas, was first presented by Hale and Moore [35]. The bvp4c solver is an algorithm that employs the Lobato IIIA implicit Runge-Kutta technique to provide numerical solutions with fourth-order accuracy. It achieves this by making finite modifications. This method provides the required precision when an estimation is made for the initial mesh points and adjustments to the step size. The investigation conducted by Waini et al. [37] shown that the bvp4c solver produced satisfactory outcomes when compared to both the direct shooting approach and Keller box method. The syntax for using the "bvp4c" solver is as follows: "sol = bvp4c (@OdeBVP, @OdeBC, solinit, options)". Here, we must decrease the higher order derivatives in relation to η. This can be accomplished by introducing the subsequent new variables:

$$f = y(1),\quad f' = y(2),\quad f'' = y(3),\quad f''' = y(4),\quad \theta = y(5),\quad \theta' = y(6)$$

$$\frac{d}{d\eta}\begin{bmatrix} y(1) \\ y(2) \\ y(3) \\ y(4) \\ y(5) \\ y(6) \end{bmatrix} = \begin{bmatrix} y(2) \\ y(3) \\ y(4) \\ \dfrac{y(2)y(3)-y(1)y(4)+\frac{Sq}{2}(3y(3)+\eta y(4))\left(a_2a_3M+\frac{a_1a_2}{Da}\right)y(3)}{a_1a_2} \\ y(6) \\ \dfrac{\frac{Sq}{2}\eta y(6)-y(1)y(6)-a_4Qy(5)-a_1a_4Ec\ y(3)^2}{\frac{a_4}{Pr}\left(a_5+\frac{4}{3}R\right)} \end{bmatrix}$$

and boundary condition are expressed as

$$y_0(1) - S,\quad y_0(2) - \lambda,\quad y_0(5) - \delta,\quad y_1(1) - \frac{Sq}{2},\quad y_1(2),\quad y_1(5) - 1$$

where y_0 is the condition at $\eta = 0$ and y_1 is the condition at $\eta = 1$

4. RESULT AND DISCUSSION

The results are computed by using bvp4c in MATLAB and visually displayed in Figs (2)-(13) for the distribution of skin friction coefficients, velocity, local Nusselt number and temperature on both the upper and bottom plates. The

Prandtl number is set at a constant value of 6.2, indicating the utilisation of water at a temperature of 25°C. The other parameters are constrained within the following ranges: $0 \leq \delta \leq 0.3$ for the temperature-ratio parameter, $0 \leq Sq \leq 1.7$ for the unsteadiness squeezing parameter, $-1.2 \leq S \leq 1.2$ for the suction/injection parameter, $-0.5 \leq \lambda \leq 2$ for the stretching/shrinking parameter, $0 \leq Da \leq 0.1$ for the porous medium parameter and $0 \leq M \leq 6$ for the magnetic parameter, $0 \leq Ec \leq 1$ for the Eckert number, $0 \leq R \leq 3$ for the thermal radiation parameter, $-0.2 \leq Q \leq 0.2$ for the heat source/sink parameter. The comparison of $f''(0)$ for the lower plate and $f''(1)$ for the upper plate with Hayat et al. [3] and Khashi'ie et al. [10] for varying values of M, S when $\lambda = 1, \phi_1 = \phi_2 = \phi_3 = 0$ is presented in Table 3. It can be seen that the results of this study are very similar to those of the two prior investigations.

Table 3. Comparison of $f''(0)$ for lower plate and $f''(1)$ for upper plate when $\lambda = 1, \phi_1 = \phi_2 = \phi_3 = 0$

M	S	Present $f''(0)$	Hayat et al. [3] $f''(0)$	Khashi'ie et al.[10] $f''(0)$	Present $f''(1)$	Hayat et al. [3] $f''(1)$	Khashi'ie et al.[10] $f''(1)$
1	0.5	-7.591617	-7.591618	-7.591617	4.739016	4.739017	4.739016
4	0.5	-8.110334	-8.110334	-8.110334	4.820251	4.820251	4.820251
4	0.6	-8.851444	-8.851444	-8.851444	5.391247	5.391248	5.391247
4	1.0	-11.948584	-11.948584	-11.948584	7.593426	7.593426	7.593426
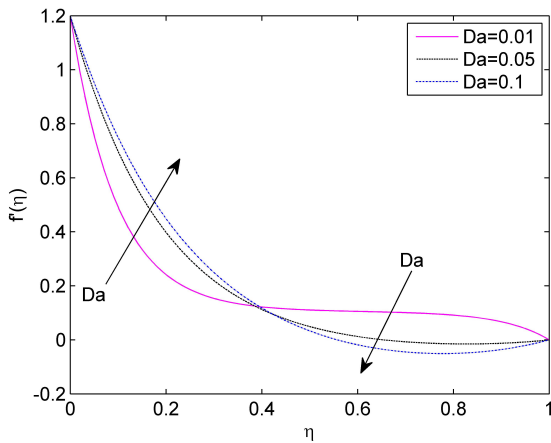
Figure 2. Effect of Da on $f'(\eta)$
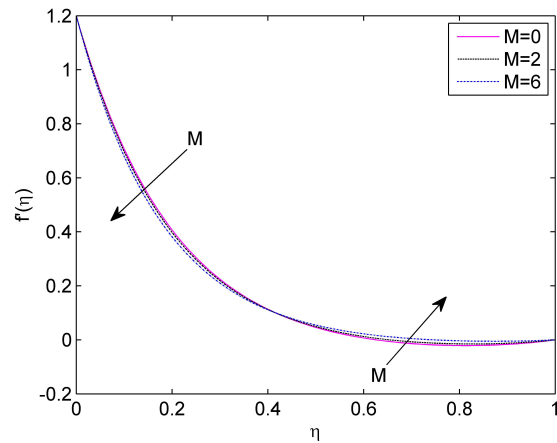
Figure 3. Effect of M on $f'(\eta)$
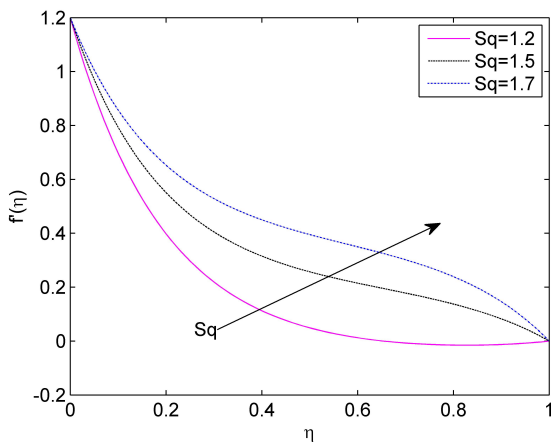
Figure 4. Effect of Sq on $f'(\eta)$
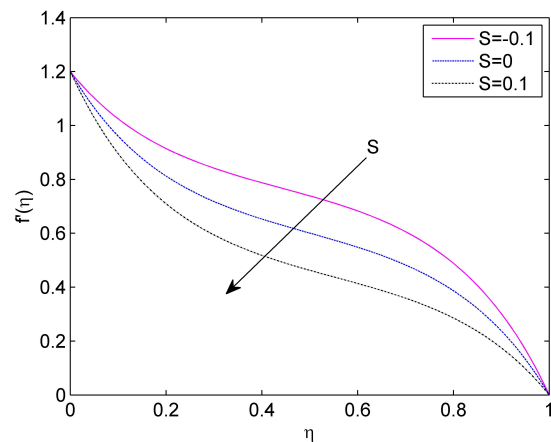
Figure 5. Effect of S on $f'(\eta)$

The parameters were set at fixed values for the computation of the results: $\delta = 0.1, Sq = 1.2, M = 2, Da = 0.05, S = 0.4, \lambda = 1.2, Ec = 0.5, R = 1, Q = 0.2, \phi_1 = \phi_2 = \phi_3 = 0.01$. The Fig. 2 displays the impact of Darcy number (Da) on velocity profile $f'(\eta)$ of the ternary hybrid nanofluid. In close proximity to the lower plate, the velocity experiences a sudden increase as the Darcy number increases. However, there is a distinct transition point at $\eta \sim 0.5$, beyond which the

velocity exhibits contrasting behaviour. The Darcy number (Da) determines the ratio of the permeability of a medium to its cross-sectional area, while permeability measures the ability of a surface to allow fluid to pass through its membrane. The rising permeability in the surrounding area of the bottom plate hinders the movement of the fluid. Consequently, a rise in the Darcy number (Da) results in velocity profiles that are closer to the upper plate due to greater flow resistance. The impact of the magnetic parameter (M) on the velocity profile is shown in Fig. 3. In close distance to the lower plate, the velocity of the ternary hybrid nanofluid decreases as the magnetic parameter increases. Similarly to Fig 2, Fig. 3 also exhibits a transition point in the vicinity of $\eta \sim 0.5$. Following this transition point, the velocity exhibits opposite behavior. The presence of a powerful magnetic field causes a significant reduction in the movement of liquids. As the magnetic field strength (M) increases, the Lorentz forces become active and cause a decrease in the flow of the liquid. The presence of a magnetic field hinders the flow and ultimately slows down the radial velocity. As seen in Fig. 4, the addition of the unsteadiness squeezing parameter(Sq) improves the velocity distribution $f'(\eta)$ for the ternary hybrid nanofluid. Due to the movement of the upper plate towards the lower plate, the squeezing effect is initiated from the higher plate. It has been observed that the velocity of the fluid increases in tandem with the squeezing parameter (Sq) as it rises higher. Fig. 5 illustrates the effect of the suction/injection parameter(S) on the velocity profile $f'(\eta)$. As seen in the figure, the application of injection results in a higher velocity than suction. Suction/injection is frequently employed as a means to prevent boundary layer separation. In this study, the application of injection results in an observed enhancement in velocity. Therefore, in this study, the injection is more efficient in delaying the separation of the boundary layer. The Fig. 6 demonstrates the impact of the shrinking/stretching parameter(λ) on the velocity profile $f'(\eta)$ for the ternary hybrid nanofluid. The velocity profile $f'(\eta)$ exhibits dual behavior with respect to shrinking/stretching parameter(λ). There is a transition point located close to $\eta \sim 0.3$. The velocity $f'(\eta)$, increases in the surrounding area of the lower plate, but beyond the transition point, the velocity $f'(\eta)$, declines. This outcome suggests that the stretching of the lower plate increases velocity in the surrounding area of the lower plate. However, when the upper plate moves towards the lower plate, the velocity behaves in the opposite way when the parameter(λ) increases.
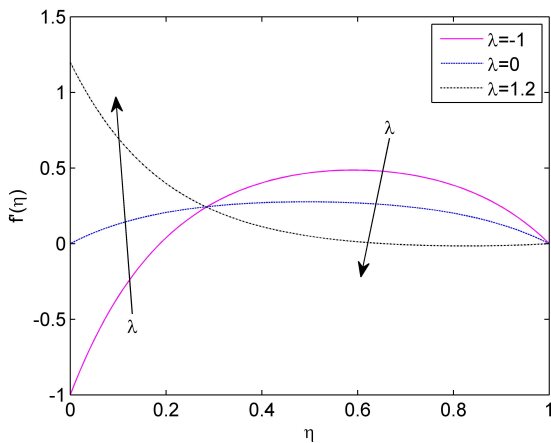
Figure 6. Effect of λ on $f'(\eta)$
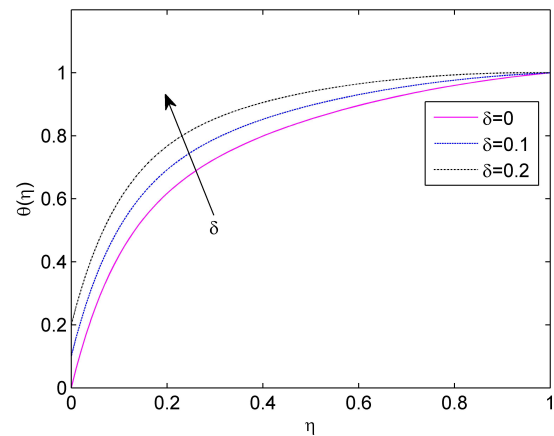
Figure 7. Effect of δ on $\theta(\eta)$
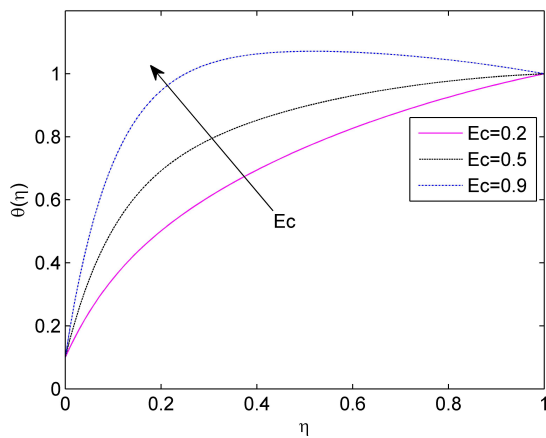
Figure 8. Effect of Ec on $\theta(\eta)$
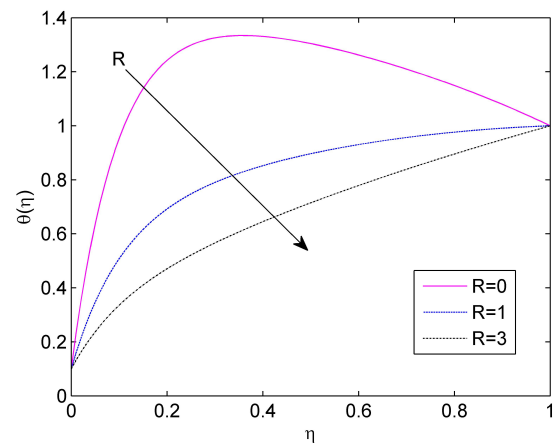
Figure 9. Effect of R on $\theta(\eta)$
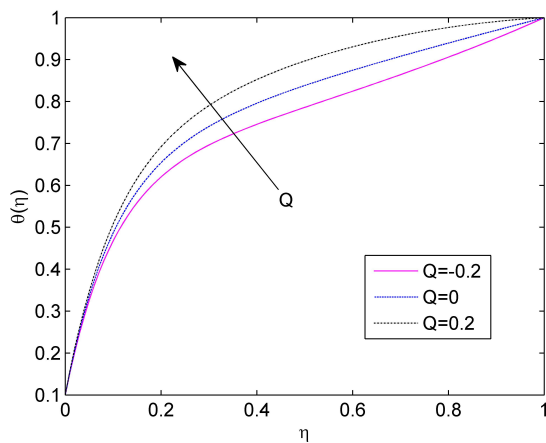
Figure 10. Effect of Q on $\theta(\eta)$
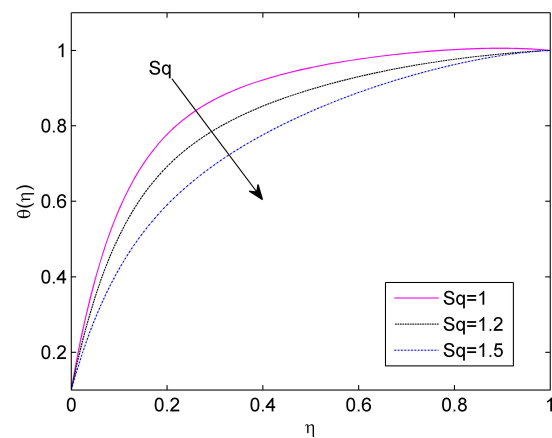
Figure 11. Effect of Sq on $\theta(\eta)$

The impact of the temperature-ratio parameter(δ) on the temperature profile $\theta(\eta)$ is shown in Fig. 7. The temperature-ratio parameter(δ) is found to increase the temperature of the ternary hybrid nanofluid due to obvious and expected reasons. In Fig 8, it is evident that the temperature of the ternary hybrid nanofluid gets raised by the Eckert number (Ec). The viscous dissipation, which is the process by which the fluid's friction causes its kinetic energy to be converted into thermal energy, becomes more important as the Eckert number(Ec) rises. The dissipation of energy causes the nanofluid to heat up, resulting in an increase in its temperature. The Fig. 9 displays that the temperature $\theta(\eta)$ of the ternary hybrid nanofluid goes down as the thermal radiation(R) goes up. Thermal radiation causes the temperature of the nanofluid to decrease by causing a net loss of energy from the fluid. This loss of energy reduces the kinetic energy of the particles inside the fluid, leading to a lower temperature. Fig. 10 demonstrates the increasing effects of temperature as the heat generation/absorption parameter (Q) increases. Greater values of a parameter (Q) result in an increase in temperature. The parameter (Q) has positive values, indicating the production of heat in the system. Higher values of (Q) correspond to greater amounts of heat being generated. Therefore, as the heat-generation parameter (Q) increases, the temperature also increases. Fig. 11 demonstrates the influence of the squeezing parameter(Sq) on the temperature profile $\theta(\eta)$. It is easy to see from the graph that as the squeezing parameter(Sq) goes up, the temperature goes down. This indicates that when the upper plate moves closer to the lower plates, it limits the spread of heat, resulting in a fall in temperature. Fig. 12 illustrates the fluctuation of the temperature,$\theta(\eta)$ for ternary hybrid nanofluid, in response to changes in the suction/injection parameter(S). An increase in parameter (S) leads to an observed rise in $\theta(\eta)$. The temperature is observed to be higher for the suction value as compared to the injection value. Suction refers to the process of extracting the layers that are detached from the border layer using suction. The fluid layers experience an increase in temperature as they gain momentum through the use of suction.
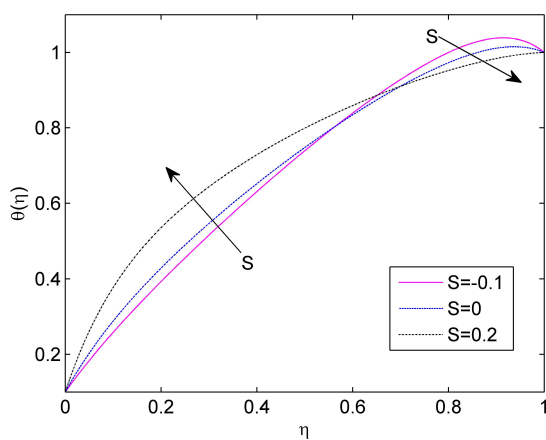
Figure 12. Effect of S on $\theta(\eta)$
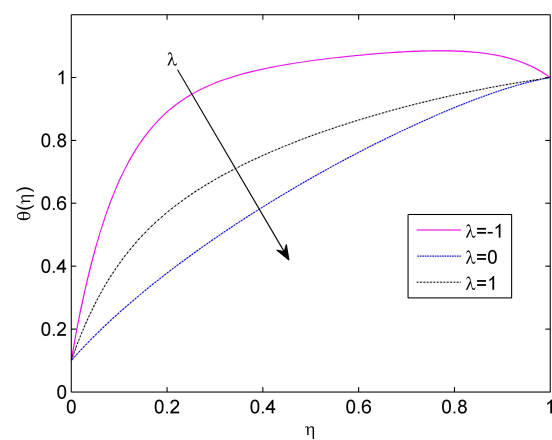
Figure 13. Effect of λ on $\theta(\eta)$

The influence of the stretching/shrinking parameter(λ) on the temperature $\theta(\eta)$ is demonstrated in Fig. 13. This model says that $\lambda = 0$ means the lower plate is still, $\lambda < 0$ means it is shrinking, and $\lambda > 0$ means it is stretching. It is observed that the velocity, $\theta(\eta)$, decreases as the values of (λ) increase. The findings suggest that the stretching of the

lower plate decreases the temperature of the flow. In addition, when the degree of shrinkage of the lower plate increases, the temperature increases.

Table 4. Skin-friction and nusselt of $f''(0)$ for upper plate when $\lambda = 1$, $\phi_1 = \phi_2 = 0$

Ec	Sq	M	Da	S	λ	R	Q	$Re_x^{1/2}C_{f_1}$	$Re_x^{1/2}C_{f_2}$	$Re_x^{-1/2}Nu_{x_1}$	$Re_x^{-1/2}Nu_{x_2}$
0.1	1.2	2	0.05	0.4	1.2	1	0.2	-6.9450	0.1994	-5.9341	-0.9706
0.5								-6.9450	0.1994	-14.8166	-0.1527
0.5	1.3	2	0.05	0.4	1.2	1	0.2	-6.5085	-0.2337	-13.4731	-0.2417
	1.5							-5.6312	-1.1046	-11.0875	-0.1442
0.5	1.2	1	0.05	0.4	1.2	1	0.2	-6.8481	0.2282	-14.7150	-0.1391
		1.5						-6.8967	0.2137	-14.7659	-0.1460
0.5	1.2	2	0.07	0.4	1.2	1	0.2	-6.3796	0.3712	-14.2404	-0.0618
			0.1					-5.9207	0.5175	-13.8064	0.0355
0.5	1.2	2	0.05	-0.1	1.2	1	0.2	-2.3816	-4.1070	-4.3122	2.5272
				0.3				-6.0088	-0.6491	-11.7957	-0.3055
0.5	1.2	2	0.05	0.4	-1	1	0.2	8.9081	-3.3656	-21.7764	2.7083
					1			-5.4744	-0.1160	-10.5985	-0.5368
0.5	1.2	2	0.05	0.4	1.2	3	0.2	-6.9450	0.1994	-16.6728	-2.5177
						5		-6.9450	0.1994	-18.9055	-4.9088
0.5	1.2	2	0.05	0.4	1.2	1	-0.2	-6.9450	0.1994	-13.7537	-1.2429
							0	-6.9450	0.1994	-14.2561	-0.7204

Table 4 presents the values of the skin friction coefficients $Re_x^{1/2}C_{f_1}$ and $Re_x^{1/2}C_{f_2}$, as well as the Nusselt numbers $Re_x^{-1/2}Nu_{x_2}$ and $Re_x^{-1/2}Nu_{x_2}$, for various combinations of parameters at the lower and upper plate. The Nusselt numbers express the rates of heat transmission between the upper and bottom plates. An increase in the Eckert number(Ec) leads to a rise in the Nusselt number for the upper plate but decreases for the lower plates. The skin friction coefficient is not influenced by Eckert number(Ec), radiation (R), and heat source (Q) at both plates, as these physical factors are independent of the velocity profile $f'(\eta)$. Increasing the squeezing parameter (Sq) enhances the heat transfer rate at the both plates. However, it reduces the skin friction coefficient at the upper plate and increases it at the lower plate. The magnetic parameter(M) causes a drop in the skin friction coefficient on both the lower and upper plates. Similarly, it leads to an decrease in the Nusselt number on the lower plate and upper plate. Observations indicate that a rise in the Darcy number(Da) leads to an increase in the skin friction coefficient on both the upper and lower plates. Likewise, it results in a increase in the Nusselt number for the both plates. The suction/injection(S) parameter reduces the skin friction coefficient on the bottom plate, but raises it on the top plate. However, the rate of heat transmission reduces at the lower and upper plates. The skin friction coefficient at the upper plate increases as the stretching parameter(λ) is increased, whereas it decreases at the lower plate. in the contrary, the rate of heat transmission increases at the bottom plate while it decreases at the top plate. Radiation(R), causes a drop in the Nusselt number at both the lower and upper plates, while the heat source(Q) results in a fall in the Nusselt number at the lower plate and an increase at the upper plate.

Table 5. Comparison of Skin friction Coefficient for lower plate

ϕ_1	Cu Nanofluid $-Re_x^{1/2}C_{f_1}$	ϕ_2	$Cu - Al_2O_3$ Hybrid Nanofluid $-Re_x^{1/2}C_{f_1}$	Change in Percentage	ϕ_3	$Cu - Al_2O_3 - SiO_2$ Ternary Hybrid Nanofluid $-Re_x^{1/2}C_{f_1}$	Change in Percentage
0.01	6.6009	0.01	6.7705	2.56%	0.01	6.9450	5.21%
0.05	7.3976		7.5841	2.52%		7.7750	5.10%
0.1	8.5447		8.7560	2.47%		8.9715	4.99%

Tables 5 and 6 present an analysis of the percentage difference between the nanofluid with hybrid nanofluid and ternary hybrid nanofluid in terms of the absolute skin friction at the top and lower plates, respectively. Moreover, we evaluate the heat transfer rate difference percentage between the nanofluid with hybrid nanofluid and ternary hybrid nanofluid at the upper and lower plates in Tables 7 and 8, respectively. The absolute skin friction of the ternary hybrid nanofluid is seen to be approximately 5% higher than that of the nanofluid at the lower plate and at most 7% higher than that of the nanofluid at the upper plate. Additionally, the rate of heat transmission of the ternary hybrid nanofluid is decreased by 3.61% at the bottom plate. However, the rate of heat transmission of the ternary hybrid nanofluid is increased by at most 209.11% at the upper plate. Observations indicate that the heat transmission rate of the ternary hybrid nanofluid is higher at the upper plate compared to the lower plate.

Table 6. Comparison of Skin friction Coefficient for upper plate

ϕ_1	Cu Nanofluid $-Re_x^{1/2}C_{f_2}$	ϕ_2	$Cu - Al_2O_3$ Hybrid Nanofluid $-Re_x^{1/2}C_{f_2}$	Change in Percentage	ϕ_3	$Cu - Al_2O_3 - SiO_2$ Ternary Hybrid Nanofluid $-Re_x^{1/2}C_{f_2}$	Change in Percentage
0.01	0.1906	0.01	0.1950	2.31%	0.01	0.1994	4.62%
0.05	0.1896		0.1949	2.79%		0.2004	5.69%
0.1	0.1966		0.2032	3.35%		0.2103	6.96%

Table 7. Comparison of Local Nusselt number for lower plate

ϕ_1	Cu Nanofluid $-Re_x^{-1/2}Nu_{x_1}$	ϕ_2	$Cu - Al_2O_3$ Hybrid Nanofluid $-Re_x^{-1/2}Nu_{x_1}$	Change in Percentage	ϕ_3	$Cu - Al_2O_3 - SiO_2$ Ternary Hybrid Nanofluid $-Re_x^{-1/2}Nu_{x_1}$	Change in Percentage
0.01	15.3716	0.01	15.0910	1.82%	0.01	14.8166	3.61%
0.05	14.3461		14.0945	1.75%		13.8468	3.48%
0.1	13.1438		12.9288	1.63%		12.7149	3.26%

Table 8. Comparison of Local Nusselt number for upper plate

ϕ_1	Cu Nanofluid $-Re_x^{-1/2}Nu_{x_2}$	ϕ_2	$Cu - Al_2O_3$ Hybrid Nanofluid $-Re_x^{-1/2}Nu_{x_2}$	Change in Percentage	ϕ_3	$Cu - Al_2O_3 - SiO_2$ Ternary Hybrid Nanofluid $-Re_x^{-1/2}Nu_{x_2}$	Change in Percentage
0.01	0.0494	0.01	0.1029	108.29%	0.01	0.1527	209.11%
0.05	0.2767		0.3306	19.47%		0.3798	37.26%
0.1	0.5622		0.6176	9.85%		0.6665	18.55%

5. CONCLUSION

The present study is a comprehensive examination of the impact of viscous dissipation and thermal radiation on the squeezing flow of a ternary hybrid nanofluid with magnetic field effect between two Parallel Plates, when a heat source/sink is present inside a porous medium. The analysis also takes into account the flow characteristics and their impact on the velocity $f'(\eta)$ and temperature $\theta(\eta)$ profiles, skin friction coefficients, and Nusselt number. The main results of the ongoing study are summarized below:

1. The velocity profile $f'(\eta)$ shows a decrease in pattern when the parameters S and λ on the upper plate and Da on the upper plate are increased. Conversely, it displays an increasing pattern with higher values of Sq and λ on the lower plate, as well as Da on the lower plate.
2. The temperature $\theta(\eta)$ decreases as the values of R, Sq and λ increase, whereas it increases with the increase of δ, Q and Ec.
3. The absolute skin friction of the ternary hybrid nanofluid is seen to be approximately 5% higher than that of the regular nanofluid at the lower plate and at most 7% higher than that of the nanofluid at the upper plate.
4. The ternary hybrid nanofluid demonstrates superior heat transfer efficiency compared to the hybrid nanofluid, while the hybrid nanofluid displays higher heat transfer efficiency than standard nanofluids at the upper plate.
5. The heat transmission rate of the ternary hybrid nanofluid is higher at the upper plate compared to the lower plate.

The future potential of ternary hybrid nanofluids, which consist of copper (Cu), aluminum oxide (Al_2O_3), and titanium dioxide (TiO_2), is significant in multiple scientific and technical fields. Ternary hybrid nanofluids provide the possibility of greatly enhancing heat transfer efficiency in various applications, such as radiators, heat exchangers and cooling devices. Improved heat transfer properties might be beneficial for use in geothermal power extraction, solar energy systems and high-temperature operations.

ORCID

 Rubul Bora, https://orcid.org/0000-0002-3164-2255; **Bidyut Boruah**, https://orcid.org/0009-0004-4978-1343

REFERENCES

[1] S.U.S. Choi, and J.A. Eastman, *Enhancing thermal conductivity of fluids with nanoparticles*, (Argonne National Lab., Argonne, IL, United States, 1995).

[2] A. Raees, H. Xu, and S.-J. Liao, "Unsteady mixed nano-bioconvection flow in a horizontal channel with its upper plate expanding or contracting," International Journal of Heat and Mass Transfer, **86**, 174-182 (2015). https://doi.org/10.1016/j.ijheatmasstransfer.2015.03.003

[3] T. Hayat, T. Muhammad, A. Qayyum, A. Alsaedi, and M. Mustafa, "On squeezing flow of nanofluid in the presence of magnetic field effects," Journal of Molecular Liquids, **213**, 179-185 (2016). https://doi.org/10.1016/j.molliq.2015.11.003

[4] T. Hayat, R. Sajjad, A. Alsaedi, T. Muhammad, and R. Ellahi, "On squeezed flow of couple stress nanofluid between two parallel plates," Results in physics, **7**, 553-561 (2017). https://doi.org/10.1016/j.rinp.2016.12.038

[5] S. Salehi, A. Nori, Kh. Hosseinzadeh, and D.D. Ganji, "Hydrothermal analysis of MHD squeezing mixture fluid suspended by hybrid nanoparticles between two parallel plates," Case Studies in Thermal Engineering, **21**, 100650 (2020). https://doi.org/10.1016/j.csite.2020.100650

[6] N. Acharya, "On the flow patterns and thermal behaviour of hybrid nanofluid flow inside a microchannel in presence of radiative solar energy," Journal of Thermal Analysis and Calorimetry, **141**(4), 1425-1442 (2020). https://doi.org/10.1007/s10973-019-09111-w

[7] N. Acharya, R. Bag, and P.K. Kundu, "Unsteady bioconvective squeezing flow with higher-order chemical reaction and second-order slip effects," Heat Transfer, **50**(6), 5538-5562 (2021). https://doi.org/10.1002/htj.22137

[8] S. Islam, A. Khan, W. Deebani, E. Bonyah, N.A. Alreshidi, and Z. Shah, "Influences of Hall current and radiation on MHD micropolar non-newtonian hybrid nanofluid flow between two surfaces," AIP Advances, **10**(5), 055015 (2020). https://doi.org/10.1063/1.5145298

[9] M.D. Ikram, M.I. Asjad, A. Akgül, and D. Baleanu, "Effects of hybrid nanofluid on novel fractional model of heat transfer flow between two parallel plates," Alexandria Engineering Journal, **60**(4), 3593-3604 (2021). https://doi.org/10.1016/j.aej.2021.01.054

[10] N.S. Khashi'ie, I. Waini, N.Md. Arifin, and I. Pop, "Unsteady squeezing flow of Cu-Al$_2$O$_3$/water hybrid nanofluid in a horizontal channel with magnetic field," Scientific reports, **11**(1), 14128 (2021). https://doi.org/10.1038/s41598-021-93644-4

[11] M. Yaseen, S.K. Rawat, A. Shafiq, M. Kumar, and K. Nonlaopon, "Analysis of heat transfer of mono and hybrid nanofluid flow between two parallel plates in a Darcy porous medium with thermal radiation and heat generation/absorption," Symmetry, **14**(9), 1943 (2022). https://doi.org/10.3390/sym14091943

[12] H.T. Rostami, M.F. Najafabadi, Kh. Hosseinzadeh, and D.D. Ganji, "Investigation of mixture-based dusty hybrid nanofluid flow in porous media affected by magnetic field using RBF method," International Journal of Ambient Energy, **43**(1), 6425-6435 (2022). https://doi.org/10.1080/01430750.2021.2023041

[13] A.R. Faisal, N.A. Shah, and T. Botmart, "Hall current and morphological effects on mhd micropolar non-newtonian tri-hybrid nanofluid flow between two parallel surfaces," Scientific Reports, **12**(1), 16608 (2022). https://doi.org/10.1038/s41598-022-19625-3

[14] I. Waini, A. Ishak, and I. Pop. "Radiative and magnetohydrodynamic micropolar hybrid nanofluid flow over a shrinking sheet with joule heating and viscous dissipation effects," Neural Computing and Applications, **34**(5), 3783-3794 (2022). https://doi.org/10.1007/s00521-021-06640-0

[15] O.A. Famakinwa, O.K. Koriko, and K.S. Adegbie, "Effects of viscous dissipation and thermal radiation on time dependent incompressible squeezing flow of CuO-Al$_2$O$_3$/water hybrid nanofluid between two parallel plates with variable viscosity," Journal of Computational Mathematics and Data Science, **5**, 100062 (2022). https://doi.org/10.1016/j.jcmds.2022.100062

[16] M. Bilal, A. El-Sayed Ahmed, R.A. El-Nabulsi, N.A. Ahammad, K.A.M. Alharbi, M.A. Elkotb, W. Anukool, and A.S.A. Zedan, "Numerical analysis of an unsteady, electroviscous, ternary hybrid nanofluid flow with chemical reaction and activation energy across parallel plates," Micromachines, **13**(6), 874 (2022). https://doi.org/10.3390/mi13060874

[17] H. Hanif, W. Jamshed, M.R. Eid, R. Ibrahim, S. Shafie, A.A. Raezah, S.M. El Din, *et al.*, "Numerical Crank-Nicolson methodology analysis for hybridity aluminium alloy nanofluid flowing based-water via stretchable horizontal plate with thermal resistive effect," Case Studies in Thermal Engineering, **42**, 102707 (2023). https://doi.org/10.1016/j.csite.2023.102707

[18] N.A.M. Noor, and S. Shafie, "Magnetohydrodynamics squeeze flow of sodium alginate-based Jeffrey hybrid nanofluid with heat sink or source," Case Studies in Thermal Engineering, **49**, 103303 (2023). https://doi.org/10.1016/j.csite.2023.103303

[19] A. Ullah, N. Fatima, K.A.M. Alharbi, S. Elattar, and W. Khan, "A numerical analysis of the hybrid nanofluid (Ag+TiO$_2$+water) flow in the presence of heat and radiation fluxes," Energies, **16**(3), 1220 (2023). https://doi.org/10.3390/en16031220

[20] N.C. Roy, and I. Pop, "Analytical investigation of transient free convection and heat transfer of a hybrid nanofluid between two vertical parallel plates," Physics of Fluids, **34**(7), 072005 (2022). https://doi.org/10.1063/5.0096694

[21] P. Jayavel, R. Katta, and R.K. Lodhi, "Numerical analysis of electromagnetic squeezing flow through a parallel porous medium plate with impact of suction/injection," Waves in Random and Complex Media, 1-24, (2022). https://doi.org/10.1080/17455030.2022.2088890

[22] K. Bhaskar, K. Sharma, and K. Bhaskar. "MHD squeezed radiative flow of Casson hybrid nanofluid between parallel plates with joule heating," International Journal of Applied and Computational Mathematics, **10**(2), 80 (2024). https://doi.org/10.1007/s40819-024-01720-w

[23] H. Maiti, and S. Mukhopadhyay, "Squeezing unsteady nanofluid flow among two parallel plates with first-order chemical reaction and velocity slip," Heat Transfer, **53**(4), 1790-1815 (2024). https://doi.org/10.1002/htj.23015

[24] B.M. Madit, J.K. Kwanza, and P.R. Kiogora, "Hydromagnetic squeezing nanofluid flow between two vertical plates in presence of a chemical reaction," Journal of Applied Mathematics and Physics, **12**(1), 126-146 (2024). https://doi.org/10.4236/jamp.2024.121011

[25] N.S. Khashi'ie, N.Md. Arifin, E.H. Hafidzuddin, and N. Wahi, "Dual stratified nanofluid flow past a permeable shrinking/stretching sheet using a non-fourier energy model," Applied sciences, **9**(10), 2124 (2019). https://doi.org/10.3390/app9102124

[26] N.S. Khashi'ie, E.H. Hafidzuddin, N.Md. Arifin, and N. Wahi, "Stagnation point flow of hybrid nanofluid over a permeable vertical stretching/shrinking cylinder with thermal stratification effect," CFD Letters, **12**(2), 80-94 (2020). https://www.akademiabaru.com/submit/index.php/cfdl/article/view/3215/2247

[27] R.S. Nath, and R.K. Deka, "Theoretical Study of Thermal and Mass Stratification Effects on MHD Nanofluid Past an Exponentially Accelerated Vertical Plate in a Porous Medium in Presence of Heat Source, Thermal Radiation and Chemical Reaction," International Journal of Applied and Computational Mathematics, 10(2), 92 (2024). https://doi.org/10.1007/s40819-024-01721-9

[28] R.S. Nath, and R.K. Deka, "Thermal and mass stratification effects on MHD nanofluid past an exponentially accelerated vertical plate through a porous medium with thermal radiation and heat source," International Journal of Modern Physics B, 2550045, (2024). https://doi.org/10.1142/S0217979225500456

[29] R.S. Nath, and R.K. Deka, "Thermal and mass stratification effects on unsteady parabolic flow past an infinite vertical plate with exponential decaying temperature and variable mass diffusion in porous medium," ZAMM-Journal of Applied Mathematics and Mechanics/Zeitschrift für Angewandte Mathematik und Mechanik, e202300475 (2024). https://doi.org/10.1002/zamm.202300475

[30] R.S. Nath, and R.K. Deka, "A Numerical Study on the MHD Ternary Hybrid Nanofluid (Cu-Al_2O_3-TiO_2/H_2O) in presence of Thermal Stratification and Radiation across a Vertically Stretching Cylinder in a Porous Medium," East European Journal of Physics, (1), 232-242 (2024). https://doi.org/10.26565/2312-4334-2024-1-19

[31] R.S. Nath, and R.K. Deka, "A Numerical Investigation of the MHD Ternary Hybrid Nanofluid (Cu-Al_2O_3-TiO_2/H_2O) Past a Vertically Stretching Cylinder in a Porous Medium with Thermal Stratification," Journal of Advanced Research in Fluid Mechanics and Thermal Sciences, **116**(1), 78-96 (2024). https://doi.org/10.37934/arfmts.116.1.7896

[32] M.V. Krishna, "Numerical investigation on steady natural convective flow past a perpendicular wavy surface with heat absorption/generation," International Communications in Heat and Mass Transfer, 139, 106517 (2022). https://doi.org/10.1016/j.icheatmasstransfer.2022.106517

[33] M.V. Krishna, and K. Vajravelu, "Rotating MHD flow of second grade fluid through porous medium between two vertical plates with chemical reaction, radiation absorption, Hall, and ion slip impacts," Biomass Conversion and Biorefinery, **14**(7), 8745-8759 (2024). https://doi.org/10.1007/s13399-022-02802-9

[34] M.V. Krishna, "Hall effects on magnetohydrodynamic rotating flow through porous medium in a parallel plate channel with various oscillations of pressure gradient," Heat Transfer, **52**(1), 236-266 (2023). https://doi.org/10.1002/htj.22693

[35] N. Hale, and D. Moore, *A sixth-order extension to the MATLAB package bvp4c of J. Kierzenka and L. Shampine*, (Oxford University Computing Laboratory, 2008).

[36] S. Rosseland, *Astrophysik und atom-theoretische Grundlagen*, (Springer-Verlag; Berlin, 1931).

[37] I. Waini, A. Ishak, and I. Pop, "Mixed convection flow over an exponentially stretching/shrinking vertical surface in a hybrid nanofluid," Alexandria Engineering Journal, **59**(3), 1881-1891 (2020). https://doi.org/10.1016/j.aej.2020.05.030

ЧИСЕЛЬНЕ ДОСЛІДЖЕННЯ СТИСКАЮЧОГО ПОТОКУ ПОТРІЙНОЇ ГІБРИДНОЇ НАНОРІДИНИ ($Cu - Al_2O_3 - TiO_2/H_2O$) МІЖ ДВОМА ПАРАЛЕЛЬНИМИ ПЛАСТИНАМИ В ПОРИСТОМУ СЕРЕДОВИЩІ ДАРСІ З В'ЯЗКОЮ ДИСИПАЦІЄЮ ТА ДЖЕРЕЛОМ ТЕПЛА

Рубул Бора, **Бідют Боруа**

Факультет математики, коледж CNB, Бокахат-785612, Ассам, Індія

Ця робота спрямована на чисельне дослідження впливу в'язкої дисипації та джерела тепла на магнітогідродинамічний стискаючий потік потрійних гібридних нанофлюїдів на водній основі між двома паралельними пластинами в пористому середовищі Дарсі. Наночастинки Cu, Al_2O_3 і TiO_2 диспергуються в базовій рідині H_2O, що призводить до створення потрійної гібридної нанорідини $Cu - Al_2O_3 - TiO_2/H_2O$. У цьому дослідженні вивчається деформація нижньої пластини, коли верхня просувається до неї. Чисельні результати обчислюються за допомогою 3-етапного методу Лобатто IIIа, який спеціально реалізовано Bvp4c у MATLAB. Вплив різних параметрів візуально проілюстровано за допомогою графіків і кількісно показано в таблицях. Вважається, що абсолютне поверхневе тертя потрійної гібридної нанорідини приблизно на 5% вище, ніж у звичайної нанорідини на нижній пластині, і щонайбільше на 7% вище, ніж у нанорідини на верхній пластині. Швидкість теплопередачі потрійної гібридної нанофлюїду вища на верхній пластині порівняно з нижньою.

Ключові слова: *теплове випромінювання; в'язке розсіювання; паралельна пластина; джерело тепла; потрійний гібридний нанофлюїд; пористе середовище Дарсі; bvp*